Fully $2\frac{1}{2}$D flow modeling of resin infusion under flexible tooling using unstructured meshes and wet and dry compaction properties

Josef F.A. Kessels [a,*], Attie S. Jonker [a], Remko Akkerman [b,1]

[a] *Department of Mechanical Engineering, North-West University, Private Bag X6001, Potchefstroom 2520, South Africa*
[b] *Faculty of Engineering Technology, Production Technology Group University of Twente, P.O. Box 217, 7500AE Enschede, The Netherlands*

Abstract

This article presents a model to simulate the RIFT process for complex $2\frac{1}{2}$D geometries in advance. Compaction and permeability experiments were carried out for two types of preform. A significant difference between dry and wet preform compaction was observed. The model takes both into account and by doing so, the general assumption, that the RIFT process can be modeled as a quasi-static process, becomes invalid. Therefore, a fully transient model is proposed, including the preform compaction flux. Experiments were carried out to validate the model. It was found that using the wet and dry preform properties leads to a good prediction of the height distributions, flow front positions and filling times.
© 2006 Elsevier Ltd. All rights reserved.

Keywords: A. Preform; C. Computational modeling; E. Resin flow

1. Introduction

The traditional method of manufacturing large, thin walled, composite structures is hand lay-up. This is a very labor and time intensive process. Therefore the labor costs are high and long pot life resins are needed. Furthermore when polyester based resins are used, styrene, a volatile organic compound, is emitted during this process. Cases have been reported where this styrene vapor had a detrimental effect on the workers. It can cause depression and fatigue and in severe cases psychiatric symptoms [1,2]. Another disadvantage is that the fiber volume fraction and void content are hard to control and hence final product properties may vary strongly [3].

Closed solid molds, as used in the resin transfer molding (RTM) process, overcome these problems, but require more expensive double matching molds. Especially for larger products, like yacht hulls, glider fuselages and bigger

wind turbine blades, the handling of the matching mold can become a serious problem. A good alternative, especially for larger parts, is resin infusion under flexible tooling (RIFT). In RIFT, the existing hand lay-up molds can be used with only minor alterations. The dry fiber mats (or preform) are draped into the female mold and then covered by a semi-flexible plastic sheet (bag). The mold and bag are sealed and put under vacuum. The resin is drawn into the mold by this vacuum and impregnates the preform. A sketch of the process can be seen in Fig. 1.

Although RIFT overcomes most of the problems of hand lay-up, like styrene emission and reproducibility, there is also a number of disadvantages. Due to the flexible bag, the preform is compressed under the vacuum pressure. This compression results in higher fiber volumes compared to hand lay-up, but also causes limited direct control over the thickness and hence final product properties. The thickness and fiber content depend on a number of variables: the compressibility and relaxation of the preform under pressure, the vacuum pressure itself and the interactions with bagging film, breather cloths and other ancillary materials [3].

---

* Corresponding author.
E-mail address: mgijfak@puk.ac.za (J.F.A. Kessels).
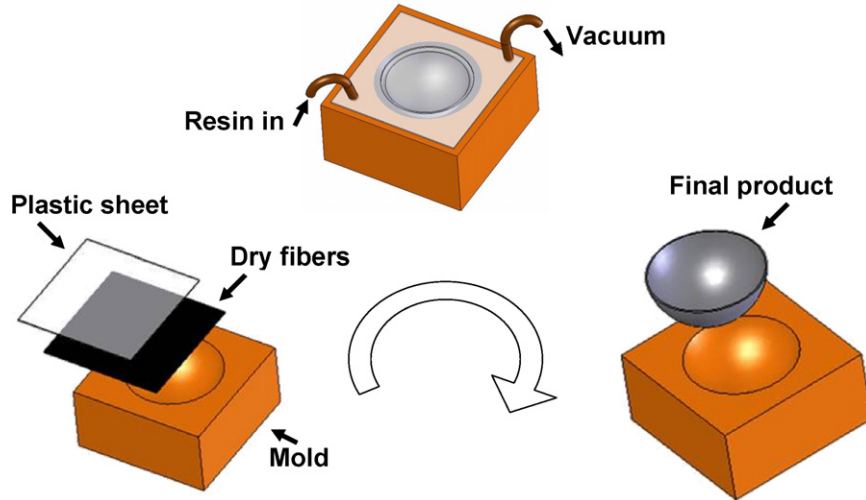[1] Tel.: +31 53 489 2566; fax: +31 53 489 3900.

Fig. 1. Schematical representation of the RIFT process.

In order to simulate the RIFT process for 3D parts, logically a 3D model would be required. Since the thickness of composite parts is often much smaller than its length and width, thin part assumptions can be used for these simulations models. For example the resin flow in the thickness direction (here denoted as z) is neglected. Therefore these models, although they describe 3D geometries, are often called $2\frac{1}{2}$ dimensional ($2\frac{1}{2}$D) flow models. In order to give a short overview of all modeling effort in the past, a number of models will be discussed here in chronological order [4–9].

The article of Gutowski et al. [4] is one of the earliest complete mathematical descriptions of the RIFT process. Like all later models, it describes the resin flow through the porous preform using Darcy's Law. According to this law the relation between the local resin flux density (also called superficial velocity), $\bar{u}$, the preform permeability K, the resin viscosity μ and the resin pressure gradient ∇P_r, can be written as

$$\bar{u} = -\frac{K}{\mu} . \nabla P_r \tag{1}$$

Gutowski et al. also assumed that the fibers make up a deformable, non-linear elastic network. Based on a control volume of length dx, width dy and height dz (see Fig. 2) Gutowski et al. derived the following resin continuity equation:

$$\frac{\partial}{\partial x}((1+\epsilon)u_x) + \frac{\partial}{\partial y}((1+\epsilon)u_y) + \frac{\partial}{\partial z}(u_z) + \frac{\partial}{\partial t}(\phi(1+\epsilon)) = 0 \tag{2}$$

In this equation ϵ is the relative change (linear strain) in z direction and ϕ is the porosity of the preform. The preform compression was modeled by assuming that the preform consists of bending beams of fibers. In later articles, this compression model is referred to as the Gutowski model. The Kozeny–Carman Theory was used to describe the relation between fiber volume fraction and permeability. These
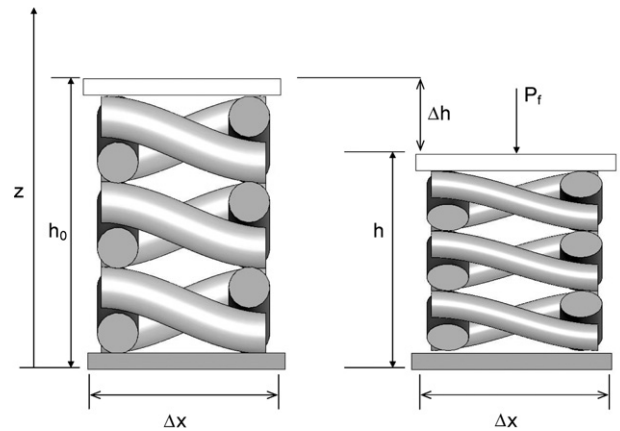

Fig. 2. The unit cell with deformable fibers.

basic equations were combined and solved for 1D and 2D compression molding and for bleeder ply molding.

Han et al. [5] used these equations to model the flow for the SCRIMP process. This process is very similar to the RIFT process, but it uses a mesh or flow channels to distribute the resin [10]. Han et al. combined the Navier–Stokes equation for the flow in the channels with Darcy's law for the flow in the preform. The preform compressibility was modeled using a power law function and the Kozeny–Carman equation was used for the permeability. A control volume method was used to solve the continuity equation where the factor $\frac{\partial}{\partial t}(\phi(1+\epsilon))$ is kept constant at every time step. This factor is defined here as the preform compaction flux term, because it actually describes the time derivative of the preform height ($\frac{\partial h}{\partial t}$). It should not be confused with the total preform compaction itself. Hammami and Gebart [6] used the same functions (however fitted to their own experimental results) but they only looked at the flow in the preform. A significant difference between the wet and dry compression behavior of the preform was found [11] but it was not used in the model. A quasi-

stationary process was assumed and therefore the preform compaction flux term was neglected, although at that time it was not proven that this approximation was valid. Andersson et al. [7] also used this assumption. They implemented the equations for the RIFT process into a commercial 3D CFD software package (CFX-4), taking wet and dry preform compaction into account. It showed that during the filling process, the thickness of the preform decreases towards the outlet. In addition a thickness minimum was observed instantly behind the resin flow-front because of a change in stiffness due to wetting of the preform. Hence the time dependency of the preform compressibility has to be considered when modeling the RIFT process. Acheson et al. [8] provided a $1\frac{1}{2}$D model to verify the correctness of the assumption to neglect the preform compaction flux term. For the materials used in this article and because only one preform compaction behavior was used, this term was very small and hence negligible. A sink term was used to model the fluid flow into the single fiber tows. RTM models were shown to give similar results if an "effective" permeability is used. However, this permeability will be different for the same material being injected under different pressures.

Based on this work, Correia et al. [9] implemented this model also, like Andersson et al., into an existing 2D/3D flow simulating software (in this case LIMS) making it possible to perform $2\frac{1}{2}$D analyses. Also in this case the preform compaction flux was neglected and the difference between wet and dry preform compressibility was not taken into account.

Looking back at all the modeling effort conducted in the past, it can be concluded that almost all models assume a quasi-stationary process and hence neglect the preform compaction flux term. Furthermore only Andersson et al. included both the wet and dry preform compressibility and showed that it could have a significant effect on the height distribution during the filling stage. Evidently the process cannot be considered quasi-static in the general case because of the relatively sudden change in height (hence height flux) at the flow front as soon as the preform wets out. Here a transient $2\frac{1}{2}$D model is presented that includes the preform compaction flux term and both the wet and dry preform compressibility. The model is verified with an analytical solution and experiments with two preform/resin systems, as specified in Table 1.

2. Principles of the model

Before we can start modeling the RIFT process, some assumptions have to be made. Firstly, the Reynolds numbers are low (laminar flow) for the resin flow, wall effects are neglected, there is no pressure gradient in the z direction and the flow can be described using Darcy's law (Eq. (1)). Secondly, the resin is incompressible and its viscosity stays constant during the filling stage.

The first assumption restricts the model to preforms with a uniform flow through the thickness. There are two situations where this occurs: The different plies have an uniform permeability over the thickness (like the 10 plies of Twill weave in Table 1) or the flow is dominated by the layer with the highest permeability. An example of the latter are preforms packs which consist of a thick flow enhancement core which is covered by just a few single plies of (woven) fabric. In such a preform the single plies of fabric are wetted instantaneously as the resin reaches the underlying core and hence the flow can be assumed to be uniform [12]. The CoreTEX fabric is an example of such a preform.

As for all other models it is assumed that in the wetted region, the total pressure is distributed over the resin, P_r, and the compactible preform, P_f, as given by the following equation:

$$P_{\text{total}} = P_{\text{atm}} - P_{\text{vac}} = P_f + P_r \tag{3}$$

In this equation P_{total}, is the total net pressure on the preform/resin system, which is the difference between the atmospheric pressure, P_{atm}, and the pressure achieved by the vacuum pump, P_{vac}.

The compaction of the preform under a pressure P_f causes a reduction of the height preform from h_0 to $h_0 - \Delta h$, as can be seen in Fig. 2. If it is assumed that the volume of the fibers in a control volume is constant, the relation between the initial (unloaded), V_{f_0}, and current fiber volume fraction, V_f, the initial, h_0, and current height, h, is given by Eq. (4)

$$(1 + \epsilon) = \frac{V_{f_0}}{V_f} = \frac{h}{h_0} \tag{4}$$

The behavior of the preform under a pressure P_f and the resulting increase of the fiber volume fraction has been studied by many authors. The compaction behavior of the materials used for this article was experimentally established using wet and dry compaction tests, similar to the ones of Hammami [11]. The preforms were put between two solid plates with known area and then compressed while the used force and height change were measured. During these experiments, it was observed that by

Table 1
Data of the used preform/resin systems

	Ten layers 280 g glass Twill	Two layers CoreTEX
Compressibility wet h (m)	$h = 0.0029186P^{-0.0559}$	$h = -5.22 \times 10^{-4}\ln(P) + 0.0090978$
Compressibility dry h (m)	$h = 0.0058786P^{-0.1013}$	$h = -5.23 \times 10^{-4}\ln(P) + 0.01023$
Uncompressed thickness h (m)	$h = 0.00287$	$h = 0.00691$
Permeability K (m²)	$K = 381.84h^{4.8866}$	$K = 8.827 \times 10^{-07}h^{1.8375}$
Used resin	Araldite LY 1564 SP	NCS 236
Viscosity of resin μ (Pa s)	0.346	0.182
Used vacuum pressure P (Pa)	87000	57500

repeating the compression test on the same sample it led to a slightly higher compression compared to the first test at equal pressures. This can be explained from a nesting effect of the material. Here the results of the first tests of every sample are used, because it is assumed that the preforms are not exposed to any pressure before the beginning of the process. Although Gutowski [4] developed a physically based model, it was found that the compaction behavior of these materials was best described, like Hammami and Gebart [6], using a power law function (see Table 1 and Fig. 3).

The permeability of the preform, K, also reduces if the preform is compressed. The permeability as a function of

the preform height (and hence fiber volume, see Eq. (4)) was experimentally established using a double-sided solid (RTM) mold with adjustable cavity height. Using flow-front sensors (which basically consist out of two copper wires which make electrical contact if the resin passes), and a weight scale, the unsaturated and saturated flow rates at different cavity heights were measured. The permeability was calculated from these flow rates using Darcy's law. Curve fitting subsequently led to an empirical relation between the permeability and the fiber content, such as the Kozeny–Carman equation. It was found, however, that a power law better fits the experimental results for the materials used here. The results are presented in Table 1 and
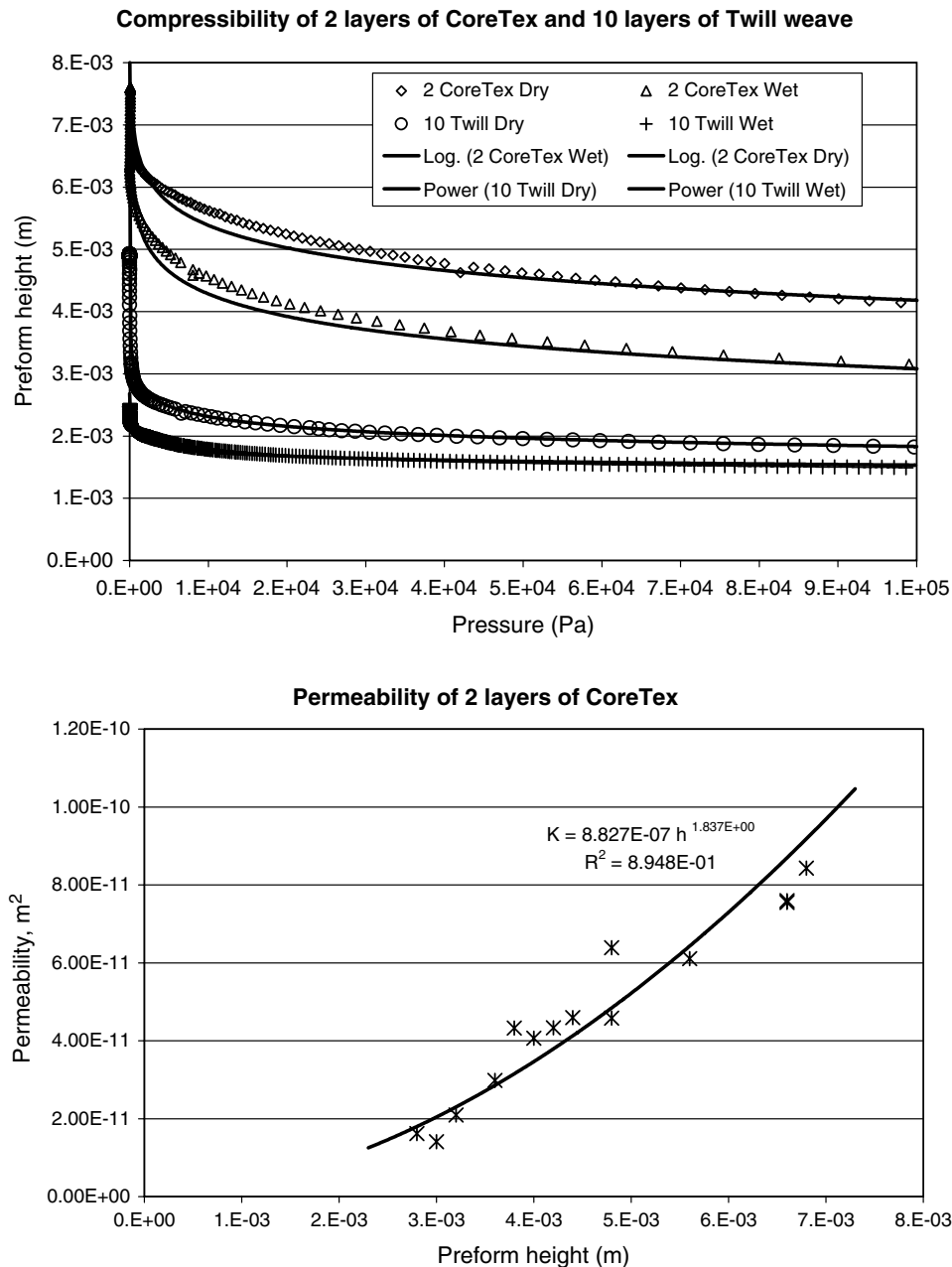

Fig. 3. Top: wet and dry compressibility behavior of CoreTEX and 10 layers of 280 g glass Twill Weave. Bottom: the measured (✳) permeability behavior and a power-law trend-line (—) of two layers of CoreTEX as a function of the preform height.

Fig. 3. A significant difference was observed between the saturated and unsaturated permeability. For example for the 10 plies of Twill weave, the unsaturated values are a factor 2.4 lower than for the saturated case. This factor is pressure independent. Hence it does not matter if the unsaturated or saturated permeability is taken to calculate the pressure field in the saturated region. This model uses therefore only the unsaturated permeability for both the saturated and unsaturated area.

We now have a description of all the factors in Eq. (1). Substituting this equation into the continuity Eq. (2) leads to the following time-dependent partial differential equation:

$$\nabla(1+\epsilon)\bar{u} + \frac{\partial}{\partial t}(\phi(1+\epsilon)) = \nabla \cdot \left(\frac{h}{h_0}\right)\left(-\frac{K}{\mu} \cdot \nabla P_r\right) + \frac{1}{h_0}\frac{\partial h}{\partial t} = 0$$
$$\Downarrow$$
$$\nabla \cdot \left(h\frac{K}{\mu} \cdot \nabla P_r\right) = \frac{\partial h}{\partial t}$$
(5)

which can be discretised using e.g. a finite volume representation.

3. Numerical model

The main advantages of the finite volume method are, that it can accommodate any type of grid, which makes it suitable for complex geometries and all terms that need to be approximated have a physical meaning and hence it is simple to understand [13,14]. The solution domain is subdivided into a finite number of contiguous control volumes (CVs), in this case triangles. At the centroid of each CV lies a computational node at which the variable values are calculated (see Fig. 4). For each of these CVs the PDE of continuity Eq. (5) can be written with the following integrals:

$$\int_A \vec{n} \cdot \left(h\frac{K}{\mu} \cdot \nabla P_r\right) dA = \int_V \frac{\partial h}{\partial t} dV$$
(6)

The left hand term represents the net rate of flow into the CV and right hand term represents the increase of the volume of the CV due to a change in height. Hence, for CV e in Fig. 4 with the net flow over its three faces, n, these integrals can be discretised as
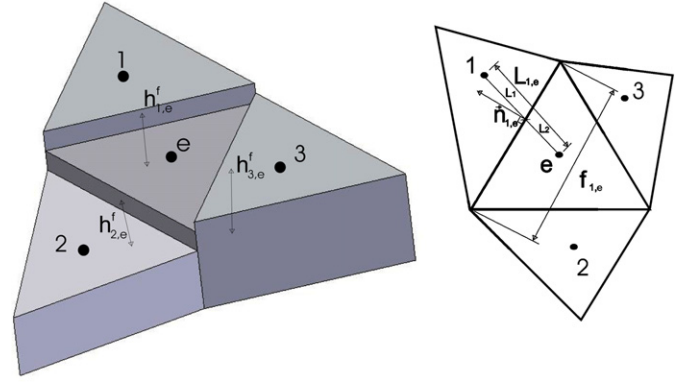

Fig. 4. Schematical representation of control volume e and its neighbors.

$$\sum_n^{1..3} C_{n,e}(P_n - P_e) = \frac{h_e^t - h_e^{t-1}}{\Delta t}V_e$$
(7)

with

$$C_{n,e} = h_{n,e}^f \frac{K_{n,e}^f}{\mu}\frac{A_{n,e}}{L_{n,e}} \cdot \vec{n}_{n,e}$$
(8)

In this equation $h_{n,e}^f$ and $K_{n,e}^f$ are, respectively, the height and the permeability of CV e at its face n, $A_{n,e}$ is the cross-section of the face side n, P_n and P_e are the pressures at respectively the neighbor CV n and the CV e itself, V_e is the volume of the CV e $L_{n,e}$ is the distance between the centroid of CV n and CV e, h_e^t is the height at the CV's centroid at time step t, and finally $\vec{n}_{n,e}$ is the normal vector of face n. The time step size, Δt, is the difference between the time at calculation step t and $t - 1$. The height at the CV faces is interpolated from the values at the centroids using a arithmetic mean [15]. For example in Fig. 4

$$h_{1,e}^f = (1-f)h_e + (f)h_1$$
(9)

with

$$f = L_2/L_{1,e}$$
(10)

The permeability at the faces is calculated from these heights using the function of Table 1. The cross-section of the face can be calculated by using the length, $f_{n,e}$, of face n of CV e : $A_{n,e} = f_{n,e} \cdot h_{n,e}^f$. The assembly of Eq. (7) for all CVs leads to the following linearized system:

$$\begin{bmatrix} (C_{i,1}+C_{j,1}+C_{k,1}) & \cdots & C_{i,1} & C_{j,1} & & C_{k,1} \\ \cdots\cdots\cdots\cdots\cdots\cdots\cdots\cdots\cdots\cdots\cdots\cdots\cdots \\ C_{1,e} & & C_{2,e} & C_{3,e} & \cdots & (C_{1,e}+C_{2,e}+C_{3,e}) \\ \cdots\cdots\cdots\cdots\cdots\cdots\cdots\cdots\cdots\cdots\cdots\cdots\cdots \end{bmatrix}\begin{bmatrix} P_1 \\ \cdots \\ P_e \\ \cdots \end{bmatrix} = \begin{bmatrix} \frac{h_1^t - h_1^{t-1}}{\Delta t}V_1 \\ \cdots\cdots\cdots \\ \frac{h_e^t - h_e^{t-1}}{\Delta t}V_e \\ \cdots \end{bmatrix}$$
(11)

Knowing that the resin pressure is equal to the vacuum pressure at the flow front and equal to the atmospheric pressure at the inlet, it is now possible to calculate the pressure field in the wetted region. This pressure field is used to calculate the height and the permeability per CV. The pressure field for the current time step is then calculated again with these new values for h and K until the difference between the previously and newly calculated pressure fields are within a certain tolerance.

4. Flow front tracking

The previous section showed that the position of the flow front is needed for the calculation of the pressure field. For the $1\frac{1}{2}D$ case, as presented in [6] and [8], the position of the flow front can be found by integrating the fluid velocity over the time t. Note that Eq. (1) only gives the resin flux density. The actual fluid velocity, $\bar{v}$ is the resin flux density divided by the porosity, ϕ:

$$\bar{v} = \frac{1}{(1-V_f)} \cdot \bar{u} = \frac{1}{\phi} \cdot \bar{u} = -\frac{K}{\mu \cdot \phi} \cdot \nabla P_r \qquad (12)$$

For the $2\frac{1}{2}D$ case, the position of the flow front is more difficult to determine. In many cases, eg. with multiple inlets, even multiple flow fronts may exist.

There are different ways to keep track of the flow front [13,14,16,17]. Here the volume of fluid technique was chosen [16,17]. This technique uses CVs as well, and in this case, the control volumes are the same as the control volumes used to calculate the pressure field. The fluid presence function, I, represents the relative volume of fluid in a cell increasing from zero for an empty volume to one for a fully saturated volume.

The main advantage of the volume of fluid technique is that only one value (the fluid presence, I) has to be stored. Furthermore also only one scalar convective equation, like other transport equations, needs to be solved. Unfortunately, it has the disadvantage that for most solution schemes, as for example first order upwind, the position of the flow front tends to smear out over several CVs. To overcome this problem, different techniques have been presented in the past as for example the donor–acceptor formulation [16]. Here a central difference scheme with variable time steps [15,18] was adopted, which is easily implemented, less diffusive and suitable for low Reynold numbers.

The fluid presence can be used to calculate the pressure field in the flow front itself. For the empty control volumes $P_r = P_{vac}$ and Eq. (5) is valid in the fully saturated volumes. A combined equation can be used for the partially filled ($0 < I < 1$) volumes [16,17].

$$I \cdot \left[\nabla \cdot h \frac{K}{\mu} \nabla P_r \right] + (I-1)[P_r] = I \cdot \left[\frac{\partial h}{\partial t} \right] + (I-1)[P_{vac}]$$

$$(13)$$

The volume of resin into each CV volume at the flow front (where $0 < I < 1$) is calculated from the velocity field at every time step. This calculation is similar to any fluid quantity in the flow (such as density, pressure, etc.) and can hence be written as [13]:

$$\frac{\partial I}{\partial t} + \bar{v} \cdot \nabla I = 0 \qquad (14)$$

Care should be taken that $I \leqslant 1$ for every CV, when solving Eq. (14) especially for the flow front CVs. If the time step, Δt, becomes too large, it can happen that for this single time step the flow front moves over more than one CV and hence I becomes larger than unity for this certain (flow front) CV. Several methods have been developed in the past as flux- and slope limiters [17] and also the previously mentioned donor–acceptor method overcomes this problem [16]. The method used here is to select at each iteration the shortest time step, Δt, to fill exactly a single CV. This method is widely used and lit gives good results [4,19]. By changing Δt to fill exactly one single CV, the term $\frac{h_e^t - h_e^{t-1}}{\Delta t} V$ of Eq. (11) changes as well. In order to prevent stability problems when solving Eq. (11) with this new Δt, a prediction of h_e^{t+1} has to be made. It would be logical to make a prediction of the new height, based on the height of the CVs at previous time steps. However, especially for the newly formed flow front CVs these data cannot be used because they had constant compacted height at all previous time steps. A different prediction is made here, based on the assumption that the right hand term of Eq. (11) stays constant. This assumption is only close to reality if $t \to \infty$ and the preform has similar dry and wet compressibility. Although not close to reality, it ensures even for the flow front CVs at least a correct order of magnitude of the height, h_e^{t+1}, with the new time step size. Therefore it provides a simple and fast way to overcome the stability problems. The approximation of h_e^t for the new time step size Δt_{new}, based on this assumption, can be written as

$$\left. \begin{array}{l} b_e = \frac{h_e^t - h_e^{t-1}}{\Delta t} V_e \\ V_e = A_e h_e^t \end{array} \right\} h_e^t = \left(h_e^{t-1} + \sqrt{(h_e^t)^2 - 4\frac{b_e \Delta t_{new}}{A_e}} \right) \Big/ 2$$

$$(15)$$

In this equation, b_e is the right hand term of Eq. (11) for CV e and A_e is the area of CV e.

We now have a full set of equations to solve the pressure, height and volume fraction distribution over the filled region and a way to keep track of the resin flow front position.

5. Simulations and experiments

The presented model was implemented within the Matlab programming environment. Before the model was verified with practical experiments, the numerical code was compared with a known analytical solution in closed

form. For the case of resin transfer molding (RTM), where no preform compression occurs, the mold filling time, t, of a 1D mold with length, x, is analytically known as [20]:

$$t = \frac{x^2(1 - V_f)\mu}{2P_\mathrm{r}K} \qquad (16)$$

The mold filling for the RTM process with a 0.2 m long mold was simulated with $V_f = 0.5$, $K/\mu = \mathrm{le}{-}13\ \mathrm{m^2/Pa\ s}$ and $P_\mathrm{total} = 100\ \mathrm{kPa}$ using 100 elements in the length direction. The top two lines of Fig. 5 show the analytical (RTM) results and the simulated ones. The position of the flow front at a certain time in the model is defined as the coordinate(s) of the center(s) of the CV(s) which has/have $I > 0$ and one or more neighboring elements with $I = 0$. All the results presented here, will have the resin inlet on the left hand side (at distance 0) and the vacuum outlet at the right hand side. It can be seen that, although the simulated values are slightly above the analytical ones, the results agree fairly well. The difference between the simulated flow front positions and analytical solution is at all times smaller than 1.5%.

A $0.2\ \mathrm{m} \times 0.2\ \mathrm{m}$ flat plate with 10 layers of 280 g glass Twill weave and a $0.45\ \mathrm{m} \times 0.45\ \mathrm{m}$ flat plate with two symmetrically stacked plies of Texglass CoreTEX were filled. The CoreTEX fabric consists of a 280 $\mathrm{g/m^2}$ glass fiber Twill weave, a 180 $\mathrm{g/m^2}$ polypropylene fiber core and a 400 $\mathrm{g/m^2}$ glass fiber chopped strand mat layer (denoted as 280 TW/ 180 PP/400 C). The resin was infused over the full width of the plate (line infusion). The position of flow front in the experiments was recorded along the centerline of the

plates. The viscosity of the resin was measured using a Brookfield viscometer. The simulated and experimental results can also be seen Fig. 5. For the 10 plies of Twill weave, the lower line shows the results if only dry preform properties are taken into account ("Dry preform properties"). The next higher line ("Without flux") shows the simulated results if the preform compaction flux term is not taken into account. The line of stars (∗) shows the results of experiment 1 ("Experiment 1") and the line of diamonds (◇) shows the results of experiment 2 ("Experiment 2"). Between those lines, the solid line shows the simulated results if dry and wet preform properties and the preform flux term are taken into account ("With flux") and the dashed line ("Wet preform properties") shows the simulated results if only wet preform properties are being used. For the two plies of CoreTEX, the same line styles are being used.

The position of the flow front depends on the viscosity of the resin, the permeability, the compressibility and the vacuum pressure level. The thickness of the preform depends, only on the compressibility and the pressure and only indirectly on the permeability (the permeability behavior only influences the pressure profile during the process). Furthermore, when the compaction behavior is known, it can be used to measure the pressure distribution in the preform indirectly. The height of the product surface during the process was measured using a laser mounted on a sliding rail. The laser scans the surface of the product along a straight line. The scanning of 0.2 m took about 0.5 s which is negligible compared to the process times. A graphite spray was sprayed on the vacuum sheet to provide a diffusive reflecting surface. The results for the 10 layers of Twill weave and a sketch of the experimental set-up can be seen in Fig. 6. The first 0.005 m of the experimental results are not shown, because in this area a pipe, used to allow a line infusion, lifts up the vacuum bag and hence gives height results which cannot be used. Finally the infusion of one side of a 2.0 m wind turbine blade was simulated and tested. The infusion pressure was 80 kPa and the CoreTEX/NCS256 preform/resin system was used. The resin inlet was at the root of the blade and the vacuum outlet at the tip. The flow front position was taken as the maximum distance between the inlet and the flow front along the x-axis (as defined in Fig. 7). The mesh with 1043 triangular CVs was generated by PATRAN and imported into the Matlab model. The calculation took 17 min on a 2.01 GHz PC with 512 MB of RAM. The results of the simulation and experiment can be seen in Fig. 7.

6. Discussion

Fig. 5 shows that if the different wet and dry preform properties are taken into account ("with flux"), the simulated results agree well with the experiments. It can also be seen that if only the dry (for the CoreTEX) or wet (for the Twill Weave) preform compaction properties are included, the simulated results also agree well. However,
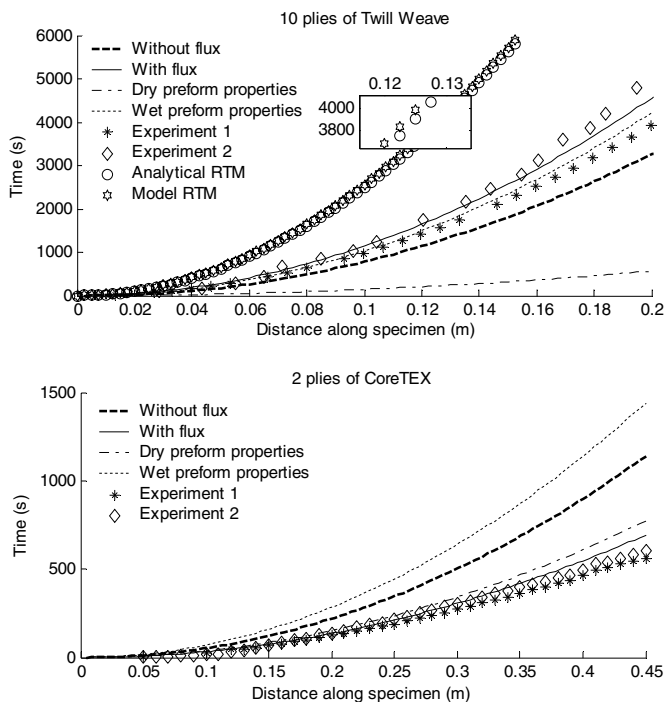

Fig. 5. Simulated, analytical and experimental results of the flow front propagation during the filling of flat plates of Twill weave (top) and CoreTEX (bottom).
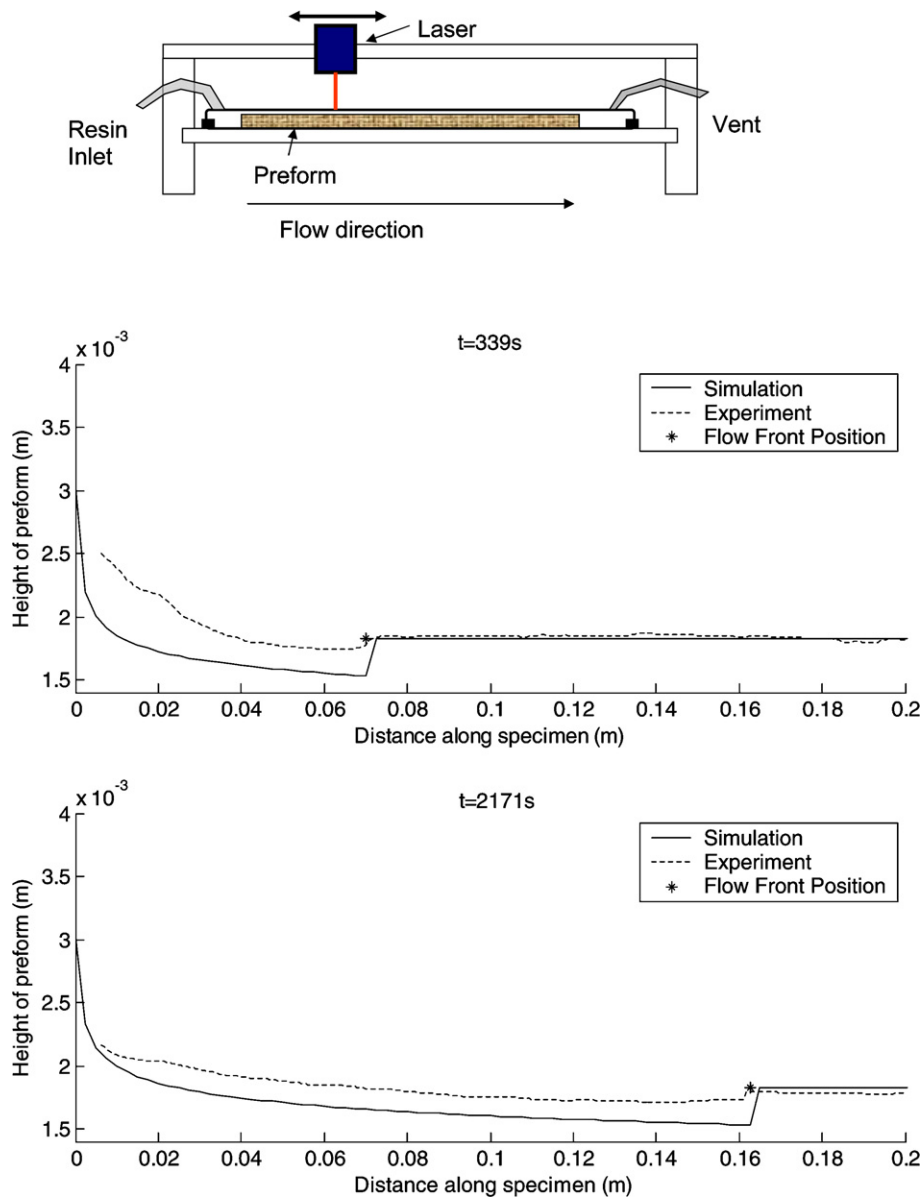
Fig. 6. Measuring the height during the filling of 10 plies of Twill weave. Top: the experimental set-up. Middle: the measured and calculated height at $t = 339$ s. Bottom: the measured and calculated height at $t = 2171$ s.

because the wet properties give good results for one material and dry properties for another material, the model cannot be simplified by using only one compaction behavior. The importance of the fully transient process model, without neglecting the flux term can also clearly be seen in Fig. 5. Fig. 6 illustrates the reason behind this. As Andersson et al. [7] already showed, a thickness minimum can be observed instantly behind the resin flow front. From this minimum the preform thickness changes quite suddenly to the larger dry compacted thickness and the flux term $\frac{\partial h}{\partial t}$ will be significant. A quasi-static process, as employed previously [4–9], is definitely not valid if different dry and wet preform properties are taken into account.

The measured values for the thickness of the wet region (the left side from the flow front) are larger than the calcu-lated ones. The thickness minimum behind the resin flow front is therefore also less pronounced than in the simulation. Possible explanations can be found in the way the compaction tests were carried out. The single plies of the preform cannot move as freely in the process compared as they can in the compaction tests. In the tests the single plies were wetted out, stacked and uniformly compressed. In the process, the fibers in the preform are still connected to the fibers in the dry region and hence transverse shear accompanies the compaction. In addition, rigid plates were used in the compression tests whereas compaction during the RIFT process is induced by the flexible bag. If we look at Fig. 2, only a small area of the fibers can actually touch these plates. Therefore the local pressure on the fibers will be much higher compared to the global pressure on the pre-
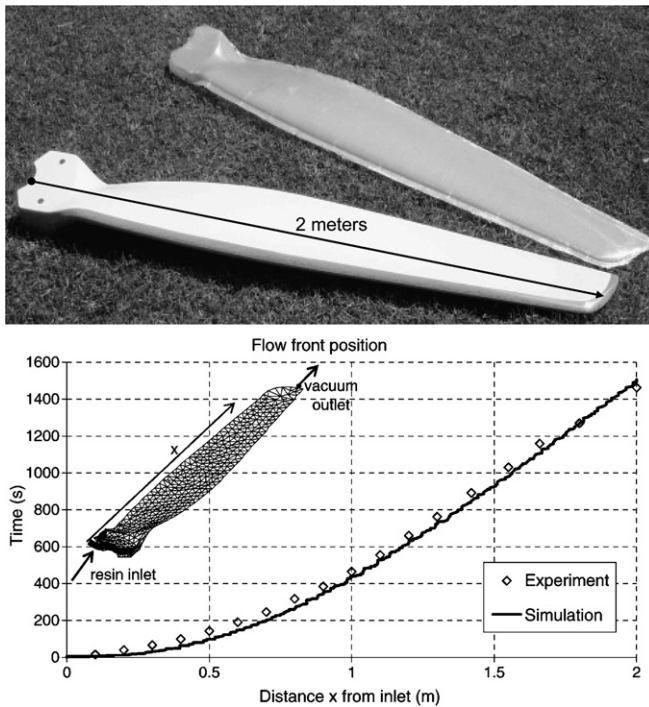
Fig. 7. Top: one side of a wind turbine blade after infusion and the final product after it is bonded to the other side and finished. Bottom: simulated and experimental results of the flow front propagation for one half of a wind turbine blade.

form. In the RIFT process the flexible bag will distribute the pressure more uniformly over the fibers. These higher local pressures could lead to a higher global preform compaction. This does not explain why there is only a difference in the wetted region between the compaction tests and the experiments. It could be that, due to a lubrication effect, wet fibers are more sensitive to local pressures than in a dry state. However, further research should validate this assumption.

Without ancillary goods, like flow channels and the flow enhancement layers, the RIFT process is quite a slow process. The experiments in this article show, that with those flow enhancement layers, like in the CoreTEX fabric, high flow front speeds can be obtained and, even without additional resin inlets, material infusion lengths of over 2 m can be reached. In this case, the flow is dominated by the layer with the highest permeability and the adjacent single plies of fabric are wetted instantaneously as the resin reaches the underlying core. If thicker or more plies are used, truly 3D flow effects will occur. The computational technique presented by Han et al. [5] could work with this model. They introduced a second fluid presence function for every CV which represents the flow in the flow enhancement layer (or even flow channels as used in SCRIMP). Using this extra function, the through-the-thickness flow at every time step can be calculated as well. In these cases there will be a flow front area where the flow enhancement layer is completely filled while the underlying woven fibers are only partially filled. This behavior cannot be predicted with the fill-one-CV-at-a-time technique, presented here. Furthermore the compaction behavior in this area will have to be determined as well.

7. Conclusion

The model presented here article uses Darcy's law, a flexible CV height and different wet and dry preform compaction properties to predict the mold filling of the RIFT process. A fluid presence function was used for flow front tracking and for the pressure prediction in the partially filled cells. The model was implemented for the use of $2\frac{1}{2}$D unstructured meshes, so complex geometries can be simulated. The preform compaction flux term was taken into account as well. This may lead to stability problems when solving the linearized system of flow equations. A stabilisation method was presented using a CV thickness prediction for a new time step size. Although this prediction was based on a rather crude assumption, it provides a simple and fast way to overcome the stability problems.

Experiments were carried out to validate the model. In some cases good predictions can be obtained with a simulation using only the dry compaction properties; in other cases the wet compaction properties lead to accurate predictions. The fully transient process model presented here appears to be generally applicable for all cases studied here.

If both preform properties are used, the results show clearly that the fully transient process model should be used, including the preform compaction flux. This does, however, increase the computational cost.

References

[1] White DM, Daniell WE, Maxewell JK, Townes BD. Psychosis following styrene exposure: a case report of neuropsychological sequelae. J Clin Exper Neuropsych 1990;12(5):798–806.
[2] Castillo L, Baldwin M, Sassine MP, Mergler D. Cumulative exposure to styrene and visual functions. Am J Ind Med 2001;39(4):351–60.
[3] Williams C, Summerscales J, Grove S. Resin infusion under flexible tooling (*RIFT*) a review. Compos Part A 1996;27A:517–24.
[4] Gutowski TG, Morigaki T, Cai Z. The consolidation of laminate composites. J Compos Mater 1987;21:172–88.
[5] Han K, Jiang S, Zhang C, Wang B. Flow modeling and simulation of *SCRIMP* for composites manufacturing. Compos Part A 2000;31: 79–86.
[6] Hammami A, Gebart BR. Analysis of the vacuum infusion molding process. Polym Compos 2000;21(1):28–40.
[7] Andersson HM, Lundström TS, Gebart BR. Numerical model for vacuum infusion manufacturing of polymer composites. Int J Numer Meth Heat Fluid Flow 2003;13(2–3):383–94.
[8] Acheson JA, Simacek P, Advani SG. The implications of fiber compaction and saturation on fully coupled *VARTM* simulation. Compos: Part A: Appl Sci Manufact 2004;35:159–69.
[9] Correia NC, Robitaille F, Long AC, Rudd CD, Simacek P, Advani SG. Use of resin transfer molding simulation to predict flow,

saturation, and compaction in the *VARTM* process. J Fluids Eng 2004;126(2):210–5.

[10] Seemann W. Plastic transfer molding techniques for the production of fiber reinforced plastic structures. US Patent No. 4,902,215, filed Mar. 30, 1989.

[11] Hammami A. Effect of reinforcement structure on compaction behavior in the vacuum infusion process. Polym Compos 2001;22(3): 337–48.

[12] Grimsley BW, Hubert P, Song X, Cano RJ, Loos AC, Pipes RB. Flow and compaction in the vacuum assisted resin transfer molding process. In: Proceedings of the 33rd international SAMPE technical conference: held in Seattle, Washington, November 4–8, 2001.

[13] Ferziger JH, Perić M. Computational methods for fluid dynamics. Springer; 1997.

[14] Versteeg HK, Malalasekera W. An introduction to computational fluid dynamics. Longman Group Ltd; 1995.

[15] Patankar Suhas V. Numerical heat transfer and fluid flow. McGraw-Hill; 1980.

[16] Hirt CW, Nichols BD. Volume of fluid (*VOF*) method for the dynamics of free boundaries. J Comput Phys 1981;39:201–25.

[17] Garcia JA, Gascón L, Chinesta F. A fixed mesh numerical method for modeling the flow in liquid composites moulding processes using a volume of fluid technique. Comput Meth Appl Mech Eng 2002;192: 877–93.

[18] Davis Stephen F. Flux difference splittings and limiters for the resolution of contact discontinuities. Appl Math Comput 1994;65: 3–18.

[19] Koorevaar A. Simulation of liquid injection molding. In: Proceedings of the SAMPE 2002 conference: held at JEC in Paris, April, 2002.

[20] Lin M, Hahn T, Huh H. A finite element simulation of resin transfer molding based on partial nodal saturation and implicit time integration. Compos Part A 1998;29A:541–50.